Available online at www.sciencedirect.com
SCIENCE DIRECT®
Computers & Fluids 33 (2004) 655–675
computers & fluids
www.elsevier.com/locate/compfluid

On the behavior of upwind schemes in the low Mach number limit: II. Godunov type schemes

Hervé Guillard [a,*], Angelo Murrone [a,b]

[a] *INRIA, BP. 93, 06902 Sophia Antipolis Cedex, France*
[b] *CEA Cadarache, 13108 Saint-Paul-Lez-Durance, France*

Received 6 June 2001; received in revised form 17 March 2003; accepted 3 July 2003

Abstract

This paper presents an analysis of Godunov scheme in the low Mach number regime. We study the Riemann problem and show that the interface pressure contains acoustic waves of order $\mathcal{O}(M_*)$ where M_* is the reference Mach number even if the initial data are well-prepared and contain only pressure fluctuations of order $\mathcal{O}(M_*^2)$. We then propose to modify the fluxes computed by Godunov type schemes by solving a preconditioned Riemann problem instead of the original one. We show that this strategy allows to recover a correct scaling of the pressure fluctuations. Numerical experiments confirm these theoretical results.

1. Introduction

Incompressible flows are a particular case of compressible ones and therefore in principle, a compressible flow solver should be able to compute these flows. Unfortunately, there are experimental evidences showing that on a fixed mesh, the solutions of the compressible flow discretized equations are not an accurate approximation of the solutions of the incompressible model (e.g. see [29]). A first analysis of this problem appeared in [23] and this question has drawn a considerable attention [1–3,7,9,26,28,30] in the recent past. Several works have tried to explain the reasons of this difficulty and to construct numerical schemes valid for all Mach numbers. Some of these works extend to the compressible regime the numerical methods used for the computation of incompressible flows. Examples of these type of methods are for instance [1] or [30]. Another approaches rely on some modifications of high order shock capturing techniques. These approaches are for instance described in [2,7,22] for Roe discretization, in [3] for the HLLE scheme

* Corresponding author.

0045-7930/$ - see front matter
doi:10.1016/j.compfluid.2003.07.001

and in [28] for Flux schemes. Their principal ingredient is the use of preconditioning techniques originally developed for steady state computations [4,21,23] that are here selectively applied only to the upwind artificial viscosity.

In [7], we have examined this technique for Roe type solvers where the numerical flux between two cells takes the following form:

$$\Phi(q_L, q_R, \mathbf{n}_{LR}) = \frac{1}{2}\left(\mathbf{F}\cdot\mathbf{n}_{LR}(q_L) + \mathbf{F}\cdot\mathbf{n}_{LR}(q_R) + \left|\frac{\partial \mathbf{F}\cdot\mathbf{n}_{LR}}{\partial q}\right|\Delta_{LR}q\right) \tag{1}$$

Here $\mathbf{n}_{LR}$ is the unit normal at the interface and $\Delta_{LR}q = q_L - q_R$ is the jump between the values q_L and q_R on each side of the interface.

By performing an asymptotic analysis of the discrete equations, we identified the limit equations satisfied by Roe discretization and showed that these limit equations support pressure fluctuations of order $\mathcal{O}(M_*)$ where M_* is the reference Mach number. Therefore, the solutions of the Roe compressible solver cannot be an accurate approximation in the low Mach number limit where pressure fluctuations scale with the *square* of the Mach number. In this paper as well as in several recent works ([23,26] for instance, see [22] for a recent survey) was put forward that this problem results from the form of the artificial viscosity tensor when the Mach number goes to zero.

In the present paper, we study the same problem for Godunov type schemes. In contrast with Roe type solvers, the flux here is of the form

$$\Phi(q_L, q_R, \mathbf{n}_{LR}) = \mathbf{F}\cdot\mathbf{n}_{LR}(q_{LR}) \tag{2}$$

where q_{LR} is the solution of an exact or approximate Riemann problem defined by the two states q_L and q_R.

Fig. 1 shows that these types of schemes exhibit the same problem of accuracy as Roe's scheme. This figure shows a sequence of computations on the same mesh of the flow around a NACA0012 airfoil while the Mach number is decreasing. In these computations, the inflow velocity is kept constant and equal to unity while the inflow pressure is increased. The figures show the normalized pressure $p - p_{min}/p_{max} - p_{min}$. As the Mach number decreases, the results become worse and the solutions do not converge to a reasonable approximation of the incompressible solution. The figures display from left to right the results obtained with Roe scheme where the flux is of the form (1), together with the results obtained by the VFRoe scheme (to be described below) and Godunov scheme where the fluxes are of the form (2). It is seen that the same results are obtained for these three upwind schemes.

Understanding the reason of this behavior is particularly interesting in the case of Godunov scheme. In Godunov scheme, the analytic expression of the flux is unknown. Therefore it is not possible to argue about the order of magnitude of the various terms of the artificial viscosity tensor. Instead the basic Riemann problem has to be considered.

Moreover, because for the initial conditions that we consider, we expect that the limit solutions of the compressible Euler equations are described by the incompressible Euler equations, a naive point of view would be to consider that the Godunov solver would give an accurate approximation of the incompressible results since in Godunov scheme, the flux computed at the interface is exact. Fig. 1 shows that this is not the case.

The reason why Godunov scheme fails to compute the incompressible limit is deeply linked to the behavior of the solutions of the Euler equations in the low Mach number regime. The crucial

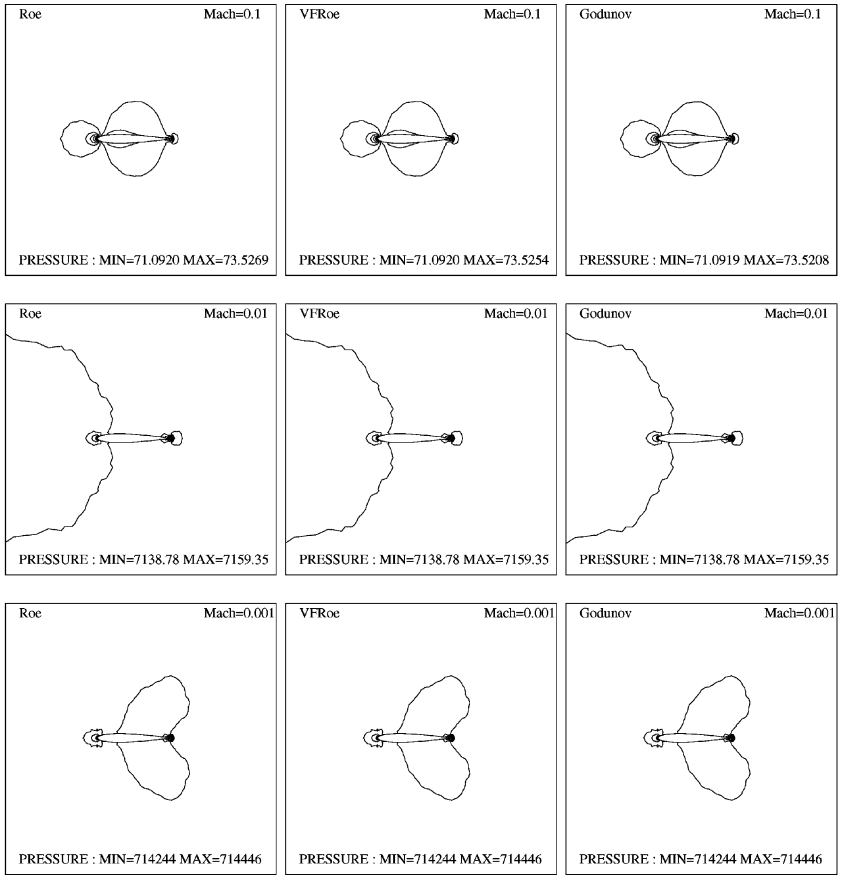

Fig. 1. Isovalues of the pressure, on a 3114 node mesh for $M_\infty = 0.1$ (top), $M_\infty = 0.01$ (middle), $M_\infty = 0.001$ (bottom) and for Roe scheme (left), VFRoe scheme (middle), Godunov scheme (right).

point to understand is that in general the strong limit solution of the compressible Euler model is not described by the incompressible Euler equations. From the work of Schochet [18] (see also [5]), this behavior for general initial data is well-understood at least for the isentropic equations and can be summarized as follows: the limit solution separates into an acoustic wave that depends on a fast time variable t/M_* plus a slow part that does not depend on this fast time variable. Moreover, the slow part does satisfy the incompressible Euler equations. If $q(\mathbf{x}, t)$ denote the solutions of the compressible model, we have as the Mach number approaches zero:

$$q(\mathbf{x}, t) = q_{\text{slow}}(\mathbf{x}, t) + q_{\text{osc}}(\mathbf{x}, t, t/M_*) + \text{HOT} \tag{3}$$

where $q_{\text{slow}}(\mathbf{x}, t)$ denote the solution of the incompressible Euler equations, $q_{\text{osc}}(\mathbf{x}, t, t/M_*)$ an oscillatory component described by an acoustic type equation and HOT stands for higher order terms.

For a restricted class of special initial data (but not in the general case) the acoustic component is not present at leading order and the solutions of the incompressible Euler equations are the strong limits of the solutions of the compressible ones as was known from some earlier results of

[8,10]. In the mathematical literature, this class of special initial data is referred to as "the well-prepared case".

For the non-isentropic model, the situation is less clear. In the well-prepared case, as shown in [17], it is known that the solutions of the incompressible model are strong limits of the solution of the compressible model. The same result is true even for general initial data in the whole space [12]. However, in the periodic case, a lot of questions remain open (see [13] for an up-to-date review of this problem).

This complex behavior explains why Godunov scheme fails to compute the incompressible limit. As we will see in Section 3, the interface values computed by a Riemann solver contain an acoustic component that carries a pressure jump of order 1 in the Mach number. This fact is in total agreement with the theoretical results recalled above. Since the initial data of the Riemann problem is a discontinuity (and thus is not well-prepared), one cannot expect that the solution of the Riemann problem will be free of acoustic component. A consequence of this fact is that the field computed by the discrete scheme results from a balance of acoustic waves instead of satisfying the equations of the incompressible model.

The plan of this work is as follows. In Section 2 we recall some known results on the behavior of the solutions of the Euler equations in the low Mach number limit. The purpose of this section is to show that the solutions of the incompressible model are only weak limits of the solutions of the compressible Euler model. For this, we introduce a simple linear model that displays the same type of behavior than the Euler equations and we indicate how the results on this model extend to the non-linear Euler model.

In Section 3, we study the solutions of the Riemann problem in the low Mach number limit. We show that even if the initial data are well-prepared and close to an incompressible field with pressure fluctuations of the order of the square of the Mach number, the solution of the Riemann problem exhibits acoustic fluctuations that scale with the Mach number. This phenomena is a direct consequence of the behavior of the compressible model for general initial data and is simply due to the fact that the projection of the initial data on piecewise constant functions creates artificial discontinuities that are responsible for the generation of pressure waves of order $\mathcal{O}(M_*)$.

For the Roe scheme, it is known that the use of preconditioning is a powerful remedy to cure the accuracy problem [2,7,22,26] the same conclusions have been reached for other types of upwind schemes as the HLLE scheme [3] or the VFFC type schemes [28]. In all these works, preconditioning is used to modify the upwind artificial viscosity tensor. Such a strategy is not possible for Godunov type schemes where the flux is expressed by (2). Thus in Section 4, we apply the idea of preconditioning directly to the Riemann solver and solve instead of the original Riemann problem a preconditioned Riemann problem. The numerical computations applied to the VFRoe schemes [11] show that preconditioning is also a powerful remedy in this context and allows accurate computations of near incompressible solutions.

2. The continuous problem

To help the understanding of the behavior of upwind schemes in the low Mach number limit, we recall in this section some known results on the continuous problem. We begin with the is-

entropic system where the mathematical theory is almost complete and restrict the discussion to the periodic case.

(Note that in the case of the whole space and even for general initial data, the results are stronger due to the decay at infinity of the energy of the acoustic component. As shown in [24] the limit solutions of the compressible equations satisfy the equations of the incompressible Euler model although uniform convergence breaks near $t = 0$.)

The isentropic Euler equations are

$$\frac{\partial \rho}{\partial t} + \mathbf{u} \cdot \nabla \rho + \rho \operatorname{div} \mathbf{u} = 0, \qquad \frac{\partial \mathbf{u}}{\partial t} + (\mathbf{u} \cdot \nabla)\mathbf{u} + \frac{1}{\rho} \nabla p = 0 \tag{4}$$

In these equations, $\mathbf{u} = (u, v)$ is a vector field and ρ a scalar field, defined on $\mathbb{R} \times T^2$ where T^2 is a two-dimensional periodic box. The pressure p is related to the density by the isentropic state law $p = A\rho^{\gamma}$ where A is a constant. To analyze this system, we first put it into a symmetric form by defining

$$\tilde{r} = \frac{2}{\gamma - 1} \sqrt{p'(\rho)} = \frac{1}{\tilde{\gamma}} \sqrt{p'(\rho)} \tag{5}$$

In term of the new variables $(r, \mathbf{u})$, the system (4) takes the form

$$\frac{\partial r}{\partial t} + \mathbf{u} \cdot \nabla r + \tilde{\gamma} r \operatorname{div} \mathbf{u} = 0, \qquad \frac{\partial \mathbf{u}}{\partial t} + (\mathbf{u} \cdot \nabla)\mathbf{u} + \tilde{\gamma} r \nabla r = 0 \tag{6}$$

Let ρ_{ref} be a typical value of the density field and define $a_{\text{ref}} = \sqrt{\gamma A \rho_{\text{ref}}^{\gamma - 1}}$ as a characteristic scale of the sound celerity. Moreover let u_{ref} be a characteristic value of the particle velocities. The reference Mach number is defined as the ratio $M_* = u_{\text{ref}}/a_{\text{ref}}$ and we are interested in the behavior of the solutions of the system (6) when this parameter goes to zero. To analyze this behavior, we first observe that up to a numerical constant of order unity, r is the speed of sound $\sqrt{p'(\rho)}$ and thus in (6) we change the variables into the following non-dimensional variables:

$$r = a_{\text{ref}}(r_0 + M_* r_1), \qquad \mathbf{u} = a_{\text{ref}}(0 + M_* \mathbf{u}_1) \tag{7}$$

where r_0 is a constant. Then, let x_{ref} be a reference length scale of the problem, we define the reference time scale as the time necessary for a fluid particle to cross the length x_{ref}, $t_{\text{ref}} = x_{\text{ref}}/u_{\text{ref}} = x_{\text{ref}}/(a_{\text{ref}} M_*)$ and then we set as non-dimensional independent variables

$$t = t_{\text{ref}} \tau, \qquad x = x_{\text{ref}} \xi \tag{8}$$

With this choice of non-dimensional variables, the system (6) takes the form

$$\frac{\partial r_1}{\partial \tau} + \mathbf{u}_1 \cdot \nabla r_1 + \tilde{\gamma} r_1 \operatorname{div} \mathbf{u}_1 + \frac{\tilde{\gamma} r_0}{M_*} \operatorname{div} \mathbf{u}_1 = 0, \qquad \frac{\partial \mathbf{u}_1}{\partial \tau} + (\mathbf{u}_1 \cdot \nabla)\mathbf{u}_1 + \tilde{\gamma} r_1 \nabla r_1 + \frac{\tilde{\gamma} r_0}{M_*} \nabla r_1 = 0 \tag{9}$$

From (9), we can expect that on very small time scales of the order $\tau = \mathcal{O}(M_*)$ (i.e. of the order of $t = x_{\text{ref}}/a_{\text{ref}}$ in dimensional units) the behavior of the solutions of (9) will be totally dominated by the acoustic part $\tilde{\gamma} r_0 (\operatorname{div} \mathbf{u}_1, \nabla r_1)^{\mathrm{t}}$ and the solutions of (9) will be close to the solutions of the system

$$\frac{\partial r_1}{\partial \theta} + \tilde{\gamma} r_0 \operatorname{div} \mathbf{u}_1 = 0, \qquad \frac{\partial \mathbf{u}_1}{\partial \theta} + \tilde{\gamma} r_0 \nabla r_1 = 0 \tag{10}$$

with $\theta = \tau/M_*$ (i.e. $\theta = a_{\text{ref}} t/x_{\text{ref}}$).

However, as the kernel of the linear acoustic operator is not void, from (9), we can also expect that the components of the solutions of (9) that are in this kernel (i.e. the incompressible part of

the solution characterized by $\operatorname{div}\mathbf{u}_1 = 0$ and $\nabla r_1 = 0$) will not be affected by the acoustic operator and will be present in the solution on large times scales. These components will satisfy the incompressible Euler equation:

$$\frac{\partial \mathbf{u}_1}{\partial \tau} + P((\mathbf{u}_1 \cdot \nabla)\mathbf{u}_1) = 0 \tag{11}$$

where P is the projection on the field of divergence free vectors. Thus in general, we can expect from the structure of the system (9) that in the low Mach number limit, its solutions will characterized by a slow (time scales of the order of $x_{\text{ref}}/u_{\text{ref}}$) incompressible component and a fast (time scales of the order of $x_{\text{ref}}/a_{\text{ref}}$) acoustic component.

As a first step in the analysis of this complex behavior, consider the following constant coefficient linear model problem obtained from (9) by a linearization around the state $(r_1, \mathbf{u}_1) = (0, \mathbf{a})$ where $\mathbf{a}$ is a constant vector. For the sake of simplicity, in the following we also set $\tilde{\gamma} r_0 = 1$:

$$\frac{\partial r_1}{\partial \tau} + \mathbf{a} \cdot \nabla r + \frac{1}{M_*} \operatorname{div}\mathbf{u}_1 = 0, \qquad \frac{\partial \mathbf{u}_1}{\partial \tau} + \mathbf{a} \cdot \nabla \mathbf{u}_1 + \frac{1}{M_*} \nabla r_1 = 0 \tag{12}$$

We write this linear system under the form

$$\frac{\partial q}{\partial \tau} + Hq + \frac{1}{M_*} Lq = 0 \tag{13}$$

where $Hq = \mathbf{a} \cdot \nabla q$ is a constant velocity linear advection operator. Writing (13) in Fourier space for the Fourier components $\hat{q}(\mathbf{k})$ of q, we get

$$\frac{\partial \hat{q}(\mathbf{k})}{\partial \tau} + \mathrm{i}\left[\hat{H}(\mathbf{k}) + \frac{1}{M_*}\hat{L}(\mathbf{k})\right]\hat{q}(\mathbf{k}) = 0 \quad \text{for } \mathbf{k} \in Z^2 \tag{14}$$

where the matrix $\hat{H}(\mathbf{k}) + 1/M_*\hat{L}(\mathbf{k})$ is equal to

$$\begin{pmatrix} \mathbf{a}\cdot\mathbf{k} & k_1/M_* & k_2/M_* \\ k_1/M_* & \mathbf{a}\cdot\mathbf{k} & 0 \\ k_2/M_* & 0 & \mathbf{a}\cdot\mathbf{k} \end{pmatrix} \tag{15}$$

and where $\mathbf{a} \cdot \mathbf{b}$ means the Euclidean inner product of the two vectors $\mathbf{a}$ and $\mathbf{b}$. This matrix is diagonalizable, its eigenvectors are

$$s_1(\mathbf{k}) = \frac{1}{\sqrt{2}}\begin{pmatrix} 1 \\ -k_1/|\mathbf{k}| \\ -k_2/|\mathbf{k}| \end{pmatrix}, \qquad s_2(\mathbf{k}) = \frac{1}{|\mathbf{k}|}\begin{pmatrix} 0 \\ -k_2 \\ k_1 \end{pmatrix}, \qquad s_3(\mathbf{k}) = \frac{1}{\sqrt{2}}\begin{pmatrix} 1 \\ k_1/|\mathbf{k}| \\ k_2/|\mathbf{k}| \end{pmatrix} \tag{16}$$

with associated eigenvalues $\lambda_1 = \mathbf{a}\cdot\mathbf{k} - \frac{|\mathbf{k}|}{M_*}$, $\lambda_2 = \mathbf{a}\cdot\mathbf{k}$ and $\lambda_3 = \mathbf{a}\cdot\mathbf{k} + \frac{|\mathbf{k}|}{M_*}$.

Therefore, the solution of (14) is

$$\begin{aligned} \hat{q}(\mathbf{k},\tau) = {} & \frac{1}{\sqrt{2}}\left(\hat{r}_1(\mathbf{k},0) - \frac{k_1}{|\mathbf{k}|}\hat{u}_1(\mathbf{k},0) - \frac{k_2}{|\mathbf{k}|}\hat{v}_1(\mathbf{k},0)\right)\mathrm{e}^{-\mathrm{i}(\mathbf{a}\cdot\mathbf{k}-|\mathbf{k}|/M_*)\tau}s_1(\mathbf{k}) + \frac{1}{|\mathbf{k}|}(-k_2\hat{u}_1(\mathbf{k},0) \\ & + k_1\hat{v}_1(\mathbf{k},0))\mathrm{e}^{-\mathrm{i}\mathbf{a}\cdot\mathbf{k}\tau}s_2(\mathbf{k}) + \frac{1}{\sqrt{2}}\left(\hat{r}_1(\mathbf{k},0) + \frac{k_1}{|\mathbf{k}|}\hat{u}_1(\mathbf{k},0) + \frac{k_2}{|\mathbf{k}|}\hat{v}_1(\mathbf{k},0)\right)\mathrm{e}^{-\mathrm{i}(\mathbf{a}\cdot\mathbf{k}+|\mathbf{k}|/M_*)\tau}s_3(\mathbf{k}) \end{aligned} \tag{17}$$

where $\hat{r}_1(\mathbf{k},0)$, $\hat{u}_1(\mathbf{k},0)$, $\hat{v}_1(\mathbf{k},0)$ are the Fourier components of the initial data. From (17) it is seen that the solution separates into a fast oscillatory component that depends on the fast time variable $\theta = \tau/M_*$

$$\hat{q}_{\mathrm{osc}}(\mathbf{k},\tau,\tau/M_*) = \frac{1}{\sqrt{2}}\left(\left(\hat{r}_1(\mathbf{k},0) - \frac{k_1}{|\mathbf{k}|}\hat{u}_1(\mathbf{k},0) - \frac{k_2}{|\mathbf{k}|}\hat{v}_1(\mathbf{k},0)\right)\mathrm{e}^{-\mathrm{i}(\mathbf{a}\cdot\mathbf{k}-|\mathbf{k}|/M_*)\tau}s_1(\mathbf{k}) + \left(\hat{r}_1(\mathbf{k},0) + \frac{k_1}{|\mathbf{k}|}\hat{u}_1(\mathbf{k},0) + \frac{k_2}{|\mathbf{k}|}\hat{v}_1(\mathbf{k},0)\right)\mathrm{e}^{-\mathrm{i}(\mathbf{a}\cdot\mathbf{k}+|\mathbf{k}|/M_*)\tau}s_3(\mathbf{k})\right) \tag{18}$$

plus a slow component that does not depend on this fast variable

$$\hat{q}_{\mathrm{slow}}(\mathbf{k},\tau) = \frac{1}{|\mathbf{k}|}(-k_2\hat{u}_1(\mathbf{k},0) + k_1\hat{v}_1(\mathbf{k},0))\mathrm{e}^{-\mathrm{i}\mathbf{a}\cdot\mathbf{k}\tau}s_2(\mathbf{k}) \tag{19}$$

In Fourier space, the kernel of the linear acoustic operator $\hat{L}(\mathbf{k})$ is the space spanned by the vector $s_2(\mathbf{k}) = (0,-k_2,k_1)^{\mathrm{t}}$. This corresponds in physical space to the space defined by

$$\ker L = \{(r_1,\mathbf{u}_1);\ r_1 = \text{constant}, \operatorname{div}\mathbf{u}_1 = 0\} \tag{20}$$

The slow component $q_{\mathrm{slow}} = \sum_{\mathbf{k}}\hat{q}_{\mathrm{slow}}(\mathbf{k},t)\mathrm{e}^{\mathrm{i}\mathbf{k}\cdot\mathbf{x}}$ is thus the projection of the solution on this space and represents the *incompressible* component of the solution. It satisfies the "incompressible system":

$$\frac{\partial q_{\mathrm{slow}}}{\partial\tau} + Hq_{\mathrm{slow}} = 0 \tag{21}$$

with initial data $q_{\mathrm{slow}}(\tau=0) = Pq(\tau=0)$ where P is the projection on $\ker L$.

From expression (18), it is seen that q_{osc} converges in the sense of distributions to 0 when $M_* \to 0$. However this is only a weak convergence and therefore except for a special class of initial data, the solution contains very fast oscillatory components that do not disappear when $M_* \to 0$: in general, even for very small M_* we have to write

$$q(\mathbf{x},t) = q_{\mathrm{slow}}(\mathbf{x},t) + q_{\mathrm{osc}}(\mathbf{x},t,t/M_*) \tag{22}$$

We now describe a special class of initial data such that we will have a strong convergence toward the incompressible limit. A necessary condition for $q(\mathbf{x},t)$ to converge strongly to the incompressible limit $q_{\mathrm{slow}}(\mathbf{x},t)$ is that $q_{\mathrm{osc}}(\mathbf{x},t,t/M_*)$ converges strongly to 0. This is not possible *except* if the initial data are close to the kernel of L. This is the case referred to as the "well-prepared case". For the isentropic Euler equations, this situation has been examined in [8,10] while for the non-isentropic model, we refer to [17].

For our model problem (12) the "well-prepared case" can be described as follows. It is clear from (17) that if

$$\begin{cases} \left(\hat{r}_1(\mathbf{k},0) - \dfrac{k_1}{|\mathbf{k}|}\hat{u}_1(\mathbf{k},0) - \dfrac{k_2}{|\mathbf{k}|}\hat{v}_1(\mathbf{k},0)\right) = \mathcal{O}(M_*) \\ \left(\hat{r}_1(\mathbf{k},0) + \dfrac{k_1}{|\mathbf{k}|}\hat{u}_1(\mathbf{k},0) + \dfrac{k_2}{|\mathbf{k}|}\hat{v}_1(\mathbf{k},0)\right) = \mathcal{O}(M_*) \end{cases} \tag{23}$$

then the oscillatory component of the solution q_{osc} converges strongly to 0 and thus the incompressible component q_{slow} is the strong limit of q as $M_* \to 0$.

In physical space, the two conditions (23) mean that the initial data have the following form:

$$\begin{cases} r_1(\mathbf{x},0) = M_* r_2(\mathbf{x},0) \\ \mathbf{u}_1(\mathbf{x},0) = \mathbf{u}_1'(\mathbf{x},0) + M_* \mathbf{u}_2(\mathbf{x},0) \end{cases} \tag{24}$$

where $r_2(\mathbf{x},0)$ is an $\mathcal{O}(1)$ scalar field, $\mathbf{u}_1'(\mathbf{x},0)$ and $\mathbf{u}_2(\mathbf{x},0)$ two $\mathcal{O}(1)$ vector fields *and* $\mathbf{u}_1'(\mathbf{x},0)$ satisfies $\operatorname{div}\mathbf{u}_1' = 0$.

Let us now return to the isentropic Euler equations (4). Although the analysis and techniques of proof are much more complex than for our linear model problem, the results are essentially the same. As proved in [18] (see also [5]), in the low Mach number limit, the solution can be written as

$$q(\mathbf{x},\tau) = q_{\text{slow}}(\mathbf{x},\tau) + q_{\text{osc}}(\mathbf{x},\tau,\tau/M_*) + \mathcal{O}(M_*) \tag{25}$$

and can be splitted into a fast acoustic component $q_{\text{osc}}(\mathbf{x},\tau,\tau/M_*)$ that depends on the fast time variable τ/M_* and a slow part $q_{\text{slow}}(\mathbf{x},\tau)$. Moreover, the slow part is a solution of the incompressible equations:

$$\operatorname{div}(\mathbf{u}_1) = 0 \tag{26a}$$

$$\rho_0\left(\frac{\partial}{\partial\tau}\mathbf{u}_1 + \operatorname{div}(\mathbf{u}_1 \otimes \mathbf{u}_1)\right) + \nabla\pi = 0 \tag{26b}$$

In general $q_{\text{slow}}(\mathbf{x},\tau)$ is only a weak limit of the solutions except for well-prepared initial data close to the kernel of L. As for the model problem, this special class of initial data is characterized by

$$\begin{cases} r_1(\mathbf{x},0) = M_* r_2(\mathbf{x},0) \\ \mathbf{u}_1(\mathbf{x},0) = \mathbf{u}_1'(\mathbf{x},0) + M_* \mathbf{u}_2(\mathbf{x},0) \quad \text{with } \operatorname{div}\mathbf{u}_1' = 0 \end{cases} \tag{27}$$

Going back to the original variables $(p,\mathbf{u})$, we see that this implies that the initial data are such that

$$\begin{cases} p(\mathbf{x},0) = \rho_{\text{ref}} a_{\text{ref}}^2 (\text{constant} + M_*^2 p_2(\mathbf{x},0)) \\ \mathbf{u}(\mathbf{x},0) = a_{\text{ref}}(0 + M_* \mathbf{u}_1(\mathbf{x},0) + M_*^2 \mathbf{u}_2(\mathbf{x},0)) \quad \text{with } \operatorname{div}\mathbf{u}_1 = 0 \end{cases} \tag{28}$$

where $p_2(\mathbf{x},0)$, $\mathbf{u}_1(\mathbf{x},0)$, $\mathbf{u}_2(\mathbf{x},0)$ are smooth, regular functions.

3. The Riemann problem in the low Mach number limit

We are interested in computing flows close to the incompressible limit. As seen in the previous section, if the initial data are well-prepared and of the form (28) with pressure fluctuations of the order of the square of the Mach number, we have strong convergence of the solution of the compressible equations to the solution of the incompressible equations. However even if the initial data do verify this assumption, the projection of these data on piecewise constant functions creates discontinuities at the interface between the cells. These discontinuities are the initial data of the Riemann problem and hence an acoustic component with pressure fluctuations of order Mach will be present in the solution of the Riemann problem.

Consider the Riemann problem defined by

$$\frac{\partial q}{\partial t}+\frac{\partial F(q)}{\partial x}=0, \qquad q(x,0)=\begin{cases} q=q_{\mathrm{L}} & \text{if } x<0 \\ q=q_{\mathrm{R}} & \text{if } x>0 \end{cases} \tag{29}$$

with

$$q=\begin{bmatrix} \rho \\ \rho u \\ \rho v \\ \rho e \end{bmatrix}, \qquad F(q)=\begin{bmatrix} \rho u \\ \rho u^2+p \\ \rho uv \\ (\rho e+p)u \end{bmatrix} \tag{30}$$

In order to make easier the description of this problem in the low Mach number limit, we recall below how to solve it in the general case. For details, one can refer for instance to [6,19]. The solution consists of four different constant states q_{L}, q^*_{L}, q^*_{R}, q_{R} connected by three waves that can be from left to right, a 1-rarefaction or a 1-shock, a contact discontinuity and a 3-rarefaction or a 3-shock. The four possible wave patterns are represented in Fig. 2.

Through a 1-rarefaction, the entropy, the tangential velocity and the quantity $u+2a/(\gamma-1)$ where a is the sound speed $\sqrt{\gamma p/\rho}$, are constant. Thus the states ρ, u, v, p that can be connected to the state ρ_{L}, u_{L}, v_{L}, p_{L} through a 1-rarefaction have to satisfy

$$\frac{p}{\rho^{\gamma}}=\frac{p_{\mathrm{L}}}{\rho_{\mathrm{L}}^{\gamma}}, \qquad u+\frac{2a}{\gamma-1}=u_{\mathrm{L}}+\frac{2a_{\mathrm{L}}}{\gamma-1} \tag{31}$$

and

$$v=v_{\mathrm{L}} \tag{32}$$

Combining the two equations (31), we obtain the 1-rarefaction curve that defines in the (u,p) plane the states that can be connected to q_{L}:

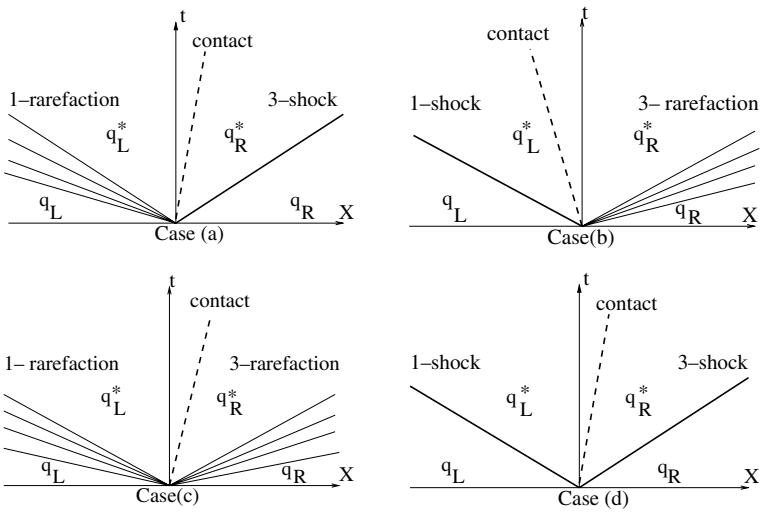

Fig. 2. The four possible wave patterns in the solution of the Riemann problem: (a) 1-rarefaction, contact, 3-shock; (b) 1-shock, contact, 3-rarefaction; (c) 1-rarefaction, contact, 3-rarefaction; (d) 1-shock, contact, 3-shock.

$$u = u_{\mathrm{L}} + \frac{2a_{\mathrm{L}}}{\gamma - 1}\left(1 - \left(\frac{p}{p_{\mathrm{L}}}\right)^{\alpha}\right) \quad \text{with } \alpha = (\gamma - 1)/2\gamma \text{ and } p < p_{\mathrm{L}} \tag{33}$$

Similarly, writing that the Riemann invariants are constant through a 3-rarefaction, we obtain the 3-rarefaction curve that defines all possible states that can be connected to q_{R} through a 3-rarefaction

$$u = u_{\mathrm{R}} - \frac{2a_{\mathrm{R}}}{\gamma - 1}\left(1 - \left(\frac{p}{p_{\mathrm{R}}}\right)^{\alpha}\right) \quad \text{with } p < p_{\mathrm{R}} \tag{34}$$

Consideration of the two curves (33) and (34) allows to compute the solution in case (c) of Fig. 2. For the other three cases, one has to take into account the occurrence of shock waves. Writing the Rankine–Hugoniot relations

$$\begin{cases} \Delta\rho u = \sigma\Delta\rho \\ \Delta\rho u^2 + p = \sigma\Delta\rho u \\ \Delta\rho uv = \sigma\Delta\rho v \\ \Delta(\rho e + p)u = \sigma\Delta\rho e \end{cases} \tag{35}$$

through the shocks, we obtain the 1-shock and 3-shock curves

$$u = u_{\mathrm{L}} - \frac{p - p_{\mathrm{L}}}{\sqrt{p + \mu^2 p_{\mathrm{L}}}}\sqrt{(1 - \mu^2)/\rho_{\mathrm{L}}} \quad \text{with } p > p_{\mathrm{L}} \tag{36}$$

$$u = u_{\mathrm{R}} + \frac{p - p_{\mathrm{R}}}{\sqrt{p + \mu^2 p_{\mathrm{R}}}}\sqrt{(1 - \mu^2)/\rho_{\mathrm{R}}} \quad \text{with } p > p_{\mathrm{R}} \tag{37}$$

where $\mu^2 = (\gamma - 1)/(\gamma + 1)$. The solution of the Riemann problem is completed by finding the values (u_*, p_*) in the states $q_{\mathrm{L}*}$ and $q_{\mathrm{R}*}$. From an algebraic point of view, this consists to find the intersection of the 1-rarefaction–1-shock curve originating from $(u_{\mathrm{L}}, p_{\mathrm{L}})$ with the 3-rarefaction–3-shock curve passing through $(u_{\mathrm{R}}, p_{\mathrm{R}})$. Except in the case of two extremely strong facing rarefactions, these two curves admit a unique intersection point which completely determines the solution of the Riemann problem.

We are now interested in the solution of this problem in the low Mach number limit. More specifically, in agreement with the results of Section 2, we consider initial data $(q_{\mathrm{L}}, q_{\mathrm{R}})$ close to a constant density incompressible flow in the following sense:

$$\begin{aligned} \rho_{\mathrm{L}} &= \rho_{\mathrm{ref}}(\rho_0 + M_*^2\rho_{\mathrm{L},2} + \cdots) \\ u_{\mathrm{L}} &= a_{\mathrm{ref}}(0 + M_* u_{\mathrm{L},1} + \cdots) \\ v_{\mathrm{L}} &= a_{\mathrm{ref}}(0 + M_* v_{\mathrm{L},1} + \cdots) \\ p_{\mathrm{L}} &= \rho_{\mathrm{ref}} a_{\mathrm{ref}}^2(p_0 + M_*^2 p_{\mathrm{L},2} + \cdots) \end{aligned} \tag{38}$$

$$\begin{aligned} \rho_{\mathrm{R}} &= \rho_{\mathrm{ref}}(\rho_0 + M_*^2\rho_{\mathrm{R},2} + \cdots) \\ u_{\mathrm{R}} &= a_{\mathrm{ref}}(0 + M_* u_{\mathrm{R},1} + \cdots) \\ v_{\mathrm{R}} &= a_{\mathrm{ref}}(0 + M_* v_{\mathrm{R},1} + \cdots) \\ p_{\mathrm{R}} &= \rho_{\mathrm{ref}} a_{\mathrm{ref}}^2(p_0 + M_*^2 p_{\mathrm{R},2} + \cdots) \end{aligned} \tag{39}$$

where ρ_{ref}, a_{ref} and $M_* = u_{\text{ref}}/a_{\text{ref}}$ are respectively a reference density, sound velocity and Mach number. Observe that these initial data are the projection on a piecewise constant field of "well-prepared" initial data of the type considered in Eq. (28) of Section 2. In particular, the pressure field does not contain fluctuations of order M_*. To find the solution of the Riemann problem in the limit $M_* \to 0$, we write the solution in the form

$$\begin{aligned}
\rho &= \rho_{\text{ref}}(\rho_0 + M_*\rho_1 + M_*^2\rho_2 + \cdots)\\
u &= a_{\text{ref}}(0 + M_* u_1 + \cdots)\\
v &= a_{\text{ref}}(0 + M_* v_1 + \cdots)\\
p &= \rho_{\text{ref}} a_{\text{ref}}^2(p_0 + M_* p_1 + M_*^2 p_2 + \cdots)
\end{aligned} \tag{40}$$

Introducing these expressions in the rarefaction and shock curves (33), (34), (36) and (37), we obtain after some calculus that in the limit $M_* \to 0$, these curves become straight lines of slopes $\pm 1/\sqrt{\gamma p_0 \rho_0}$:

$$\begin{aligned}
&\text{1-rarefaction} \quad u_1 = u_{\text{L},1} - \frac{1}{\sqrt{\gamma p_0 \rho_0}} p_1 \quad \text{for } p_1 < 0\\
&\text{1-shock} \quad\quad\ u_1 = u_{\text{L},1} - \frac{1}{\sqrt{\gamma p_0 \rho_0}} p_1 \quad \text{for } p_1 > 0\\
&\text{3-rarefaction} \quad u_1 = u_{\text{R},1} + \frac{1}{\sqrt{\gamma p_0 \rho_0}} p_1 \quad \text{for } p_1 < 0\\
&\text{3-shock} \quad\quad\ u_1 = u_{\text{R},1} + \frac{1}{\sqrt{\gamma p_0 \rho_0}} p_1 \quad \text{for } p_1 > 0
\end{aligned} \tag{41}$$

As shown in Fig. 3, out of the four possible wave patterns displayed in Fig. 2, only the 1-rarefaction–3-rarefaction (when $u_{\text{R},1} - u_{\text{L},1} > 0$) and 1-shock–3-shock (when $u_{\text{R},1} - u_{\text{L},1} < 0$) solutions are possible.

For these two cases, the computation of the intersection point of the curves (41) gives

$$u_1 = (u_{\text{L},1} + u_{\text{R},1})/2, \qquad p_1 = -\sqrt{\gamma p_0 \rho_0}\,\Delta u_1/2 \tag{42}$$

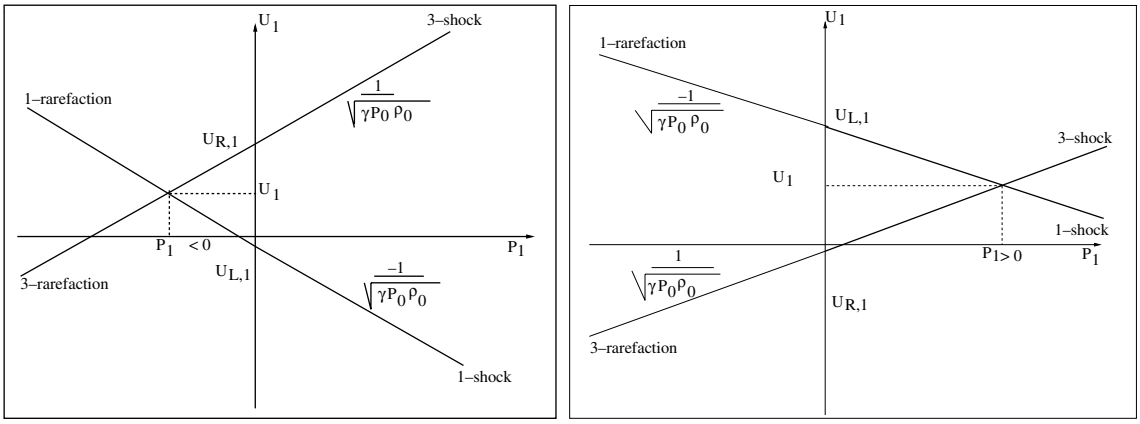

Fig. 3. Intersection of rarefaction curves for $u_{\text{R},1} - u_{\text{L},1} > 0$ (left) and shock curves for $u_{\text{R},1} - u_{\text{L},1} < 0$ (right).

with $\Delta u_1 = \Delta_{RL} u_1 = u_{R,1} - u_{L,1}$. Therefore, it is seen that even if the initial data are of the form (38) and (39) with $p_{L,1} = p_{R,1} = 0$, the interface pressure contains a fluctuation of order M_*:

$$p = \rho_{ref} a_{ref}^2 \left(p_0 - \frac{M_*}{2} \sqrt{\gamma p_0 \rho_0} \Delta u_1 + \cdots \right) \tag{43}$$

Actually, this pressure fluctuation is purely of acoustic origin. The shock curves of (41) are the Rankine–Hugoniot relations for an acoustic system and (42) is in fact the solution of the *linear acoustic* problem defined in Eq. (10) or in term of the variables u_1, p_1 by

$$\frac{\partial}{\partial t} \begin{pmatrix} u_1 \\ p_1 \end{pmatrix} + \begin{pmatrix} 0 & 1/\rho_0 \\ \gamma p_0 & 0 \end{pmatrix} \frac{\partial}{\partial x} \begin{pmatrix} u_1 \\ p_1 \end{pmatrix} = 0 \tag{44}$$

Therefore, the flux computed at the interface instead of being an approximation of the "incompressible flux" is to leading order the flux coming from an *acoustic* problem generated by the artificial discontinuities at the interfaces between the cells.

To illustrate this analysis, we compare in Fig. 4 the solution of the Riemann problem (29) and the asymptotic expression (42) for initial data of the form (38) and (39) defined by

$$\begin{cases} \rho_L = 1 \\ u_L = 1 \\ v_L = 1 \\ p_L = 10\,001 \end{cases} \quad \text{and} \quad \begin{cases} \rho_R = 1 \\ u_R = 1.75 \text{ or } 0.25 \\ v_R = 1.45 \\ p_R = 10\,001.85 \end{cases} \tag{45}$$

The reference Mach number for this case is of order 10^{-2}. In Fig. 4, the left plots display the case of a two rarefaction solution (when $u_R > u_L$) while the right plots show the case of a two shock solution (when $u_R < u_L$). Observe that in the two cases, the pressure jump between the two initial states is extremely small (of the order of 0.01%) but the velocity jump creates an extremely large variation of the interface pressure.

From an examination of the Riemann problem in the limit $M_* \to 0$, we can therefore conclude that even if the initial data are close to a constant density incompressible field, the field computed by the Godunov solver contains, after one time step, acoustic pressure waves of order M_* that are much larger than the pressure fluctuations due to the incompressible component. These acoustic components remain present in the following time steps and the equilibrium state of the discrete equations (if it exists) can be described as a balance of acoustic waves instead of representing an approximation of an incompressible field. In Appendix A, we present this limit system, the reader will notice the close resemblance of this system with the limit equations obtained from an asymptotic analysis of the Roe scheme that we have presented in [7].

4. The effect of preconditioning

For Roe type schemes, we have shown in [7] that for very subsonic flows a clear improvement of the accuracy can be obtained by modifying the numerical flux (1) in the following way:

$$\Phi(q_L, q_R, \mathbf{n}_{LR}) = \frac{1}{2} \left(\mathbf{F} \cdot \mathbf{n}_{LR}(q_L) + \mathbf{F} \cdot \mathbf{n}_{LR}(q_R) + P^{-1} \left| P \frac{\partial \mathbf{F} \cdot \mathbf{n}_{LR}}{\partial q} \right| \Delta_{LR} q \right) \tag{46}$$

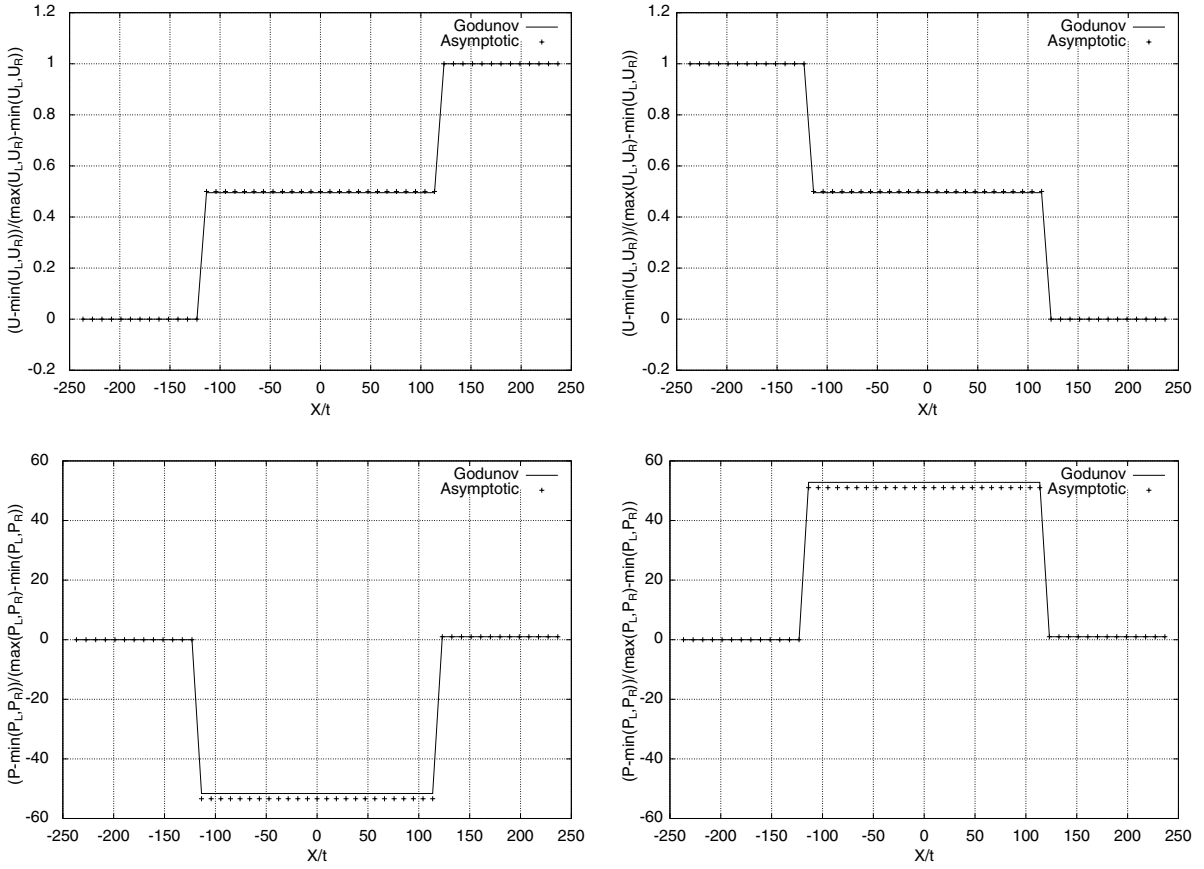

Fig. 4. Comparison between Godunov solver and asymptotic analysis for $u_R > u_L$ (left) and for $u_R < u_L$ (right).

where P is a preconditioning matrix. In this section, we propose a similar strategy to overcome the accuracy problem encountered by Godunov type schemes.

More specifically, we will apply preconditioning to the VFRoe class of schemes that we describe now. The VFRoe schemes [11] use a flux of the form

$$\Phi(q_L, q_R, \mathbf{n}_{LR}) = \mathbf{F} \cdot \mathbf{n}_{LR}(q_{LR}) \tag{47}$$

where q_{LR} is a state computed by the solution of a Riemann problem between the two states q_L, q_R. If this Riemann problem is defined by the non-linear Euler equations, the scheme defined by (47) is simply Godunov scheme. However, from a computational point of view, it may be interesting to define this Riemann problem by a linearized problem between the two states (q_L, q_R):

$$\frac{\partial \tilde{q}}{\partial t} + \langle A \rangle \frac{\partial \tilde{q}}{\partial x} = 0, \qquad \tilde{q}(x,0) = \begin{cases} \tilde{q} = \tilde{q}_L & \text{if } x < 0 \\ \tilde{q} = \tilde{q}_R & \text{if } x > 0 \end{cases} \tag{48}$$

where $\langle A \rangle$ is a constant matrix and $\tilde{q}$ can be the conservative variables q or any other set of independent variables. Here, for instance, we will use the "entropic" variables $\tilde{q} = (p, u, v, s)^t$ and define $\langle A \rangle$ by

$$\langle A\rangle = \begin{bmatrix} \langle u\rangle & \gamma\langle p\rangle & 0 & 0 \\ 1/\langle\rho\rangle & \langle u\rangle & 0 & 0 \\ 0 & 0 & \langle u\rangle & 0 \\ 0 & 0 & 0 & \langle u\rangle \end{bmatrix} \tag{49}$$

where $\langle\cdot\rangle = ((\cdot)_L + (\cdot)_R)/2$ denote the arithmetic average between $\tilde{(\cdot)}_L$ and $\tilde{(\cdot)}_R$. Thus in (47), q_{LR} are the conservative variables corresponding to the solutions $\tilde{q}_{LR}$ of the linearized Riemann problem (48). An asymptotic analysis of this upwind scheme similar to the analysis presented in Section 3 yields the same conclusions as for Godunov scheme. It shows that the interface pressure is given by expression (43) and thus that the pressure field contains fluctuations of order Mach.

In the spirit of the preconditioning of Roe scheme (46), we propose to modify the interface flux $\Phi(q_L, q_R, \mathbf{n}_{LR}) = \mathbf{F}\cdot\mathbf{n}_{LR}(q_{LR})$ by computing q_{LR} as the solution of a *preconditioned* Riemann problem. More specifically, in (47) we take q_{LR} as the solution of the preconditioned problem:

$$\frac{\partial\tilde{q}}{\partial t} + P\langle A\rangle\frac{\partial\tilde{q}}{\partial x} = 0, \qquad \tilde{q}(x,0) = \begin{cases} \tilde{q} = \tilde{q}_L & \text{if } x < 0 \\ \tilde{q} = \tilde{q}_R & \text{if } x > 0 \end{cases} \tag{50}$$

where P is the preconditioning matrix proposed in [20],

$$P = \begin{bmatrix} \beta^2 & 0 & 0 & 0 \\ 0 & 1 & 0 & 0 \\ 0 & 0 & 1 & 0 \\ 0 & 0 & 0 & 1 \end{bmatrix} \tag{51}$$

with β a parameter of the order of the Mach number: $\beta = M_*\beta_1$ with $\beta_1 = \mathcal{O}(1)$.

We proceed now to show that the interface pressure solution of the *preconditioned* Riemann problem (50) does not contain fluctuations of order M_* if the initial pressure contains only pressure fluctuations of order M_*^2. The left and right states are then defined by

$$\begin{aligned} \rho_L &= \rho_{ref}(\rho_{L,0} + M_*\rho_{L,1} + M_*^2\rho_{L,2} + \cdots) \\ u_L &= a_{ref}(0 + M_* u_{L,1} + \cdots) \\ v_L &= a_{ref}(0 + M_* v_{L,1} + \cdots) \\ p_L &= \rho_{ref}a_{ref}^2(p_0 + M_*^2 p_{L,2} + \cdots) \end{aligned} \tag{52}$$

$$\begin{aligned} \rho_R &= \rho_{ref}(\rho_{R,0} + M_*\rho_{R,1} + M_*^2\rho_{R,2} + \cdots) \\ u_R &= a_{ref}(0 + M_* u_{R,1} + \cdots) \\ v_R &= a_{ref}(0 + M_* v_{R,1} + \cdots) \\ p_R &= \rho_{ref}a_{ref}^2(p_0 + M_*^2 p_{R,2} + \cdots) \end{aligned} \tag{53}$$

Note that in (52) and (53), we allow the presence of density discontinuities of order $\mathcal{O}(1)$ but that the pressure jump between the left and right states is of order M_*^2.

To obtain an explicit expression for the solution of (50), we diagonalize the matrix $\langle A\rangle$. Its eigenvalues are given by

$$\lambda_1 = \left[(1+\beta^2)\langle u\rangle - \sqrt{X}\right]/2, \qquad \lambda_2 = \lambda_3 = \langle u\rangle, \qquad \lambda_4 = \left[(1+\beta^2)\langle u\rangle + \sqrt{X}\right]/2 \tag{54}$$

with $X = [(1-\beta^2)\langle u\rangle]^2 + 4\beta^2\gamma\langle p\rangle/\langle\rho\rangle$ and the associated eigenvectors R_k are

$$R_1 = \begin{bmatrix} 1 \\ \dfrac{\lambda_1 - \beta^2\langle u\rangle}{\beta^2\gamma\langle p\rangle} \\ 0 \\ 0 \end{bmatrix}, \qquad R_2 = \begin{bmatrix} 0 \\ 0 \\ 0 \\ 1 \end{bmatrix}, \qquad R_3 = \begin{bmatrix} 0 \\ 0 \\ 1 \\ 0 \end{bmatrix}, \qquad R_4 = \begin{bmatrix} 1 \\ \dfrac{\lambda_4 - \beta^2\langle u\rangle}{\beta^2\gamma\langle p\rangle} \\ 0 \\ 0 \end{bmatrix} \tag{55}$$

Finally, let us introduce the coordinates $\alpha_k(\Delta_{\mathrm{RL}}\tilde{q})$ of the jump $\Delta_{\mathrm{RL}}\tilde{q} = \tilde{q}_{\mathrm{R}} - \tilde{q}_{\mathrm{L}}$ in the basis of the eigenvectors R_k

$$\begin{aligned} &\alpha_1 = -\frac{(\lambda_1 - \langle u\rangle)\Delta p + \beta^2\gamma\langle p\rangle\Delta u}{\sqrt{X}}, \qquad \alpha_2 = \Delta S \\ &\alpha_3 = \Delta v, \qquad \alpha_4 = \frac{(\lambda_4 - \langle u\rangle)\Delta p + \beta^2\gamma\langle p\rangle\Delta u}{\sqrt{X}} \end{aligned} \tag{56}$$

Then, the solution of (50) is given by four constant states $\tilde{q}_{\mathrm{L}}$, $\tilde{q}^*_{\mathrm{L}}$, $\tilde{q}^*_{\mathrm{R}}$, $\tilde{q}_{\mathrm{R}}$ defined by

$$\tilde{q}(x,t) = \begin{cases} \tilde{q}_{\mathrm{L}} & \text{for } x/t < \lambda_1 \\ \tilde{q}^*_{\mathrm{L}} = \tilde{q}_{\mathrm{L}} + \alpha_1 R_1 & \text{for } \lambda_1 < x/t < \lambda_2 \\ \tilde{q}^*_{\mathrm{R}} = \tilde{q}_{\mathrm{R}} - \alpha_4 R_4 & \text{for } \lambda_2 < x/t < \lambda_4 \\ \tilde{q}_{\mathrm{R}} & \text{for } \lambda_4 > x/t \end{cases} \tag{57}$$

Using the expressions of the left and right eigenvectors (56) and (55), together with the asymptotic expansions (52) and (53), we obtain the following asymptotic expressions for the two states $\tilde{q}^*_{\mathrm{L}}$, $\tilde{q}^*_{\mathrm{R}}$ (note that the value of u and p are equal in the two states $\tilde{q}^*_{\mathrm{L}}$, $\tilde{q}^*_{\mathrm{R}}$):

$$\begin{aligned} u_* = a_{\mathrm{ref}}\Bigg(&0 + M_*\left(\langle u_1\rangle - \frac{\langle u_1\rangle}{2\sqrt{X_0}}\Delta u_1 - \frac{\Delta p_2}{\langle\rho_0\rangle\sqrt{X_0}}\right) \\ &+ M_*^2\left(\langle u_2\rangle - \frac{\langle u_1\rangle}{2\sqrt{X_0}}\Delta u_2 + (\cdots)\Delta u_1 + \frac{\langle\rho_1\rangle\Delta p_2}{\langle\rho_0\rangle\sqrt{X_0}} + (\cdots)\Delta p_2\right) + \cdots\Bigg) \\ p^* = \rho_{\mathrm{ref}}a^2_{\mathrm{ref}}&\left(p_0 + M_*^2\left(\langle p_2\rangle - \frac{\beta_1^2\gamma p_0}{\sqrt{X_0}}\Delta u_1 + \frac{\langle u_1\rangle}{2\sqrt{X_0}}\Delta p_2\right) + \cdots\right) \end{aligned} \tag{58}$$

where $X_0 = (\langle u_1\rangle)^2 + 4\beta_1^2\gamma p_0/\langle\rho_0\rangle$, $\langle\cdot\rangle = ((\cdot)_{\mathrm{L}} + (\cdot)_{\mathrm{R}})/2$ denotes the arithmetic average and $(\cdots)$ stands for some complex terms that are not explicited here.

The values of the densities and tangential velocities are given by

$$\begin{aligned} \rho^*_{\mathrm{L}} &= \rho_{\mathrm{ref}}\left(\rho_{\mathrm{L},0} + M_*\rho_{\mathrm{L},1} + M_*^2\left(\rho_{\mathrm{L},2} - \frac{\beta_1^2\rho_{\mathrm{L},0}}{\sqrt{X_0}}\Delta u_1 + \frac{\rho_{\mathrm{L},0}\langle u_1\rangle}{2\gamma p_0\sqrt{X_0}}\Delta p_2 + \frac{\rho_{\mathrm{L},0}}{2\gamma p_0}\Delta p_2\right) + \cdots\right) \\ v^*_{\mathrm{L}} &= v_{\mathrm{L}} \\ \rho^*_{\mathrm{R}} &= \rho_{\mathrm{ref}}\left(\rho_{\mathrm{R},0} + M_*\rho_{\mathrm{R},1} + M_*^2\left(\rho_{\mathrm{R},2} - \frac{\beta_1^2\rho_{\mathrm{R},0}}{\sqrt{X_0}}\Delta u_1 + \frac{\rho_{\mathrm{R},0}\langle u_1\rangle}{2\gamma p_0\sqrt{X_0}}\Delta p_2 - \frac{\rho_{\mathrm{R},0}}{2\gamma p_0}\Delta p_2\right) + \cdots\right) \\ v^*_{\mathrm{R}} &= v_{\mathrm{R}} \end{aligned} \tag{59}$$

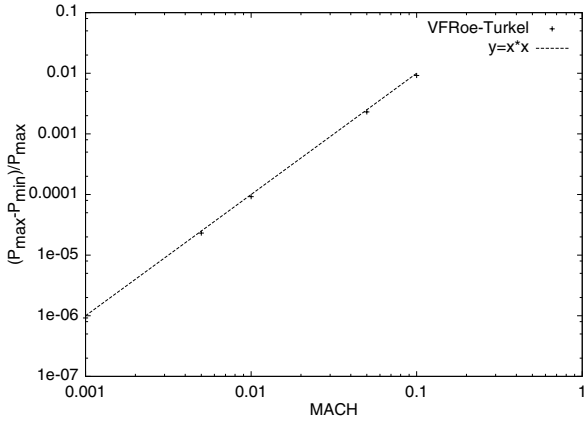

Fig. 5. Pressure fluctuations vs inflow Mach number; for comparison the curve $y = x^*x$ is displayed.

From expression (58), it is seen that the interface pressure is free of fluctuations of order Mach.

Now, let us return to the numerical experiments that we have presented in the introduction. Fig. 6 presents the pressure fields for the same three decreasing Mach numbers as in Fig. 1. We see, that in contrast to the results obtained with the original fluxes, the solution converge to a unique solution.

Fig. 5 presents the pressure fluctuations with respect to the Mach number. As implied by expression (58), the pressure fluctuations scale exactly with the square of the Mach number in agreement with the behavior of the continuous equations in the case of well-prepared initial data.

5. Conclusion

Using an asymptotic analysis of Godunov scheme, we have exhibited the mechanism that prevents this type of approximation to compute near incompressible flows. The trouble comes from the fact that the interface pressure computed by the Riemann solver contains pressure fluctuations of order Mach even if the initial data that define the Riemann problem contain fluctuations that scale with the square of the Mach number. This fact is deeply linked to the behavior of the solutions of the Euler equations at low Mach number: if the initial data are not well-prepared, then, in addition to the incompressible component, the solutions of the Euler equations contain also an extremely fast acoustic part. This acoustic part is computed by the discrete scheme that reacts to the artificial discontinuities due to the projection of the initial data on piecewise constants by creating acoustic waves at the interface between the cells.

We also show that as in the case of Roe scheme [7], this situation can be controlled by modifying the numerical fluxes with the help of preconditioning techniques. More specifically, we propose to change the original Riemann problem by a *preconditioned* Riemann problem. We apply this strategy to a VFRoe scheme. In this latter case, we show both theoretically and numerically that the solution of the preconditioned Riemann problem possesses pressure fluctuations of the correct magnitude.

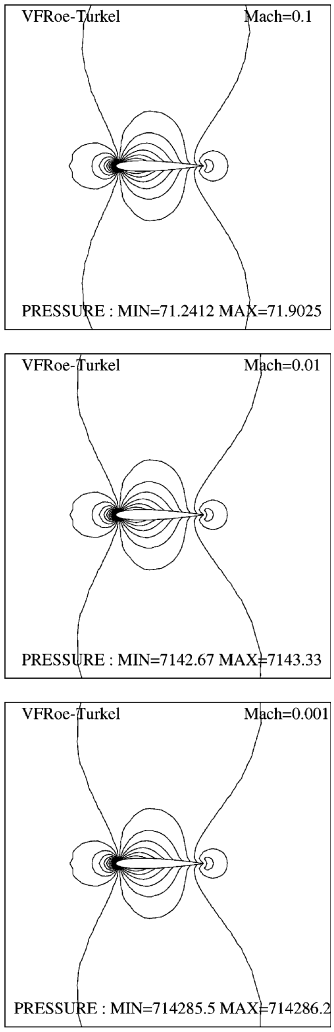

Fig. 6. Isovalues of the pressure, on a 3114 node mesh for $M_\infty = 0.1$ (top), $M_\infty = 0.01$ (middle), $M_\infty = 0.001$ (bottom).

Preconditioned compressible solvers [2,3,7,22,26] are able to deal with the singularity of the Euler equations in the low Mach number regime. Comparisons with incompressible and low Mach number solvers show the excellent behavior of these methods (see e.g. [14–16,26,27]. However, in our opinion, the reason of this good behavior remains unclear. As mentioned by van Leer and Darmofal in [25] the beneficial influence of preconditioning on the accuracy of compressible solvers in the low Mach number regime was an unexpected side effect. In this paper, as a first step in the analysis of these methods, we have shown that the most obvious result of preconditioning consists of removing the fluctuations of order Mach in the interface pressures. Thus, in some sense, the preconditioned solvers suppress the unwanted acoustic waves generated by the interface discontinuities. It will remain to prove that the resulting fluxes provide a good approximation of the incompressible system. While there is experimental evidence showing that this is indeed the case, the theoretical proof of this fact remains to be found.

Acknowledgements

The work of Angelo Murrone has been supported by a grant of the "Conseil Régional" of PACA région and the DTP/STH/LMTA of CEA Cadarache. Angelo Murrone wishes to acknowledge the support of M. Grandotto (CEA Cadarache), P. Gubernatis (CEA Cadarache) and R. Saurel (IUSTI Marseille). He would also like to thank his family for their constant support as well as C. Viozat for her precious advice.

Appendix A

Here, as in Section 3, we consider the limit solution of the Riemann problem (29) in order to identify the limit system satisfied by the discrete unknowns. In Section 3, we have shown that even if the initial data are "well-prepared" and of the form (38) and (39), the solution after one time step contains pressure waves of order M_*. Therefore, we have to consider more general initial data than (38) and (39), i.e. we have to consider the case where the initial data although still characterized by a low Mach number are not well-prepared. In addition, since the incompressible Euler model supports density discontinuities, we also allow in the initial data the possibility to have $\mathcal{O}(1)$ density discontinuities. Thus the two states q_{L} and q_{R} are assumed to have the following form:

$$\begin{aligned}
\rho_{\mathrm{L}} &= \rho_{\mathrm{ref}}(\rho_{\mathrm{L},0} + M_*\rho_{\mathrm{L},1} + M_*^2\rho_{\mathrm{L},2} + \cdots)\\
u_{\mathrm{L}} &= a_{\mathrm{ref}}(0 + M_* u_{\mathrm{L},1} + M_*^2 u_{\mathrm{L},2} + \cdots)\\
v_{\mathrm{L}} &= a_{\mathrm{ref}}(0 + M_* v_{\mathrm{L},1} + M_*^2 v_{\mathrm{L},2} + \cdots)\\
p_{\mathrm{L}} &= \rho_{\mathrm{ref}} a_{\mathrm{ref}}^2(p_0 + M_* p_{\mathrm{L},1} + M_*^2 p_{\mathrm{L},2} + \cdots)
\end{aligned} \tag{A.1}$$

and

$$\begin{aligned}
\rho_{\mathrm{R}} &= \rho_{\mathrm{ref}}(\rho_{\mathrm{R},0} + M_*\rho_{\mathrm{R},1} + M_*^2\rho_{\mathrm{R},2} + \cdots)\\
u_{\mathrm{R}} &= a_{\mathrm{ref}}(0 + M_* u_{\mathrm{R},1} + M_*^2 u_{\mathrm{R},2} + \cdots)\\
v_{\mathrm{R}} &= a_{\mathrm{ref}}(0 + M_* v_{\mathrm{R},1} + M_*^2 v_{\mathrm{R},2} + \cdots)\\
p_{\mathrm{R}} &= \rho_{\mathrm{ref}} a_{\mathrm{ref}}^2(p_0 + M_* p_{\mathrm{R},1} + M_*^2 p_{\mathrm{R},2} + \cdots)
\end{aligned} \tag{A.2}$$

As in Section 3, we introduce these asymptotic expansions in the shock and rarefaction curves. It is easily seen that again these curves degenerate into straight lines of slopes $-1/\sqrt{\gamma p_0 \rho_{\mathrm{L},0}}$ and $+1/\sqrt{\gamma p_0 \rho_{\mathrm{R},0}}$. However, because $p_{\mathrm{L},1}$ and $p_{\mathrm{R},1}$ are not zero, the four possible waves pattern of Fig. 2 can occur. Moreover, due to the $\mathcal{O}(1)$ density discontinuities, the speeds of sound are not equal on the two sides of the contact discontinuity. However, in the four possible cases, the intersection of the shock and rarefaction curves gives

$$\begin{aligned}
u^* &= a_{\mathrm{ref}}\left(0 + M_*\left(\frac{\sqrt{\rho_{\mathrm{L},0}}u_{L,1} + \sqrt{\rho_{\mathrm{R},0}}u_{\mathrm{R},1}}{\sqrt{\rho_{\mathrm{L},0}} + \sqrt{\rho_{\mathrm{R},0}}} - \frac{1}{\sqrt{\gamma p_0}}\frac{\Delta p_1}{\sqrt{\rho_{\mathrm{L},0}} + \sqrt{\rho_{\mathrm{R},0}}}\right) + M_*^2\cdots\right)\\
p^* &= \rho_{\mathrm{ref}} a_{\mathrm{ref}}^2\left(p_0 + M_*\left(\frac{\sqrt{\rho_{\mathrm{R},0}}p_{L,1} + \sqrt{\rho_{\mathrm{L},0}}p_{\mathrm{R},1}}{\sqrt{\rho_{\mathrm{L},0}} + \sqrt{\rho_{\mathrm{R},0}}} - \sqrt{\gamma p_0}\frac{\sqrt{\rho_{\mathrm{L},0}\rho_{\mathrm{R},0}}}{\sqrt{\rho_{\mathrm{L},0}} + \sqrt{\rho_{\mathrm{R},0}}}\Delta u_1\right) + M_*^2\cdots\right)
\end{aligned} \tag{A.3}$$

where $\Delta(\cdot) = \Delta_{RL}(\cdot) = (\cdot)_R - (\cdot)_L$.

The values of the density and tangential velocities on the two sides of the contact discontinuity are given by

$$\begin{aligned}
\rho_L^* &= \rho_{ref}\left(\rho_{L,0} + M_*\left(\rho_{L,1} - \rho_{L,0}\frac{\sqrt{\rho_{L,0}\rho_{R,0}}}{\sqrt{\rho_{L,0}}+\sqrt{\rho_{R,0}}}\frac{\Delta u_1}{\sqrt{\gamma p_0}} + \frac{\rho_{L,0}\sqrt{\rho_{L,0}}}{\sqrt{\rho_{L,0}}+\sqrt{\rho_{R,0}}}\frac{\Delta p_1}{\gamma p_0}\right) + M_*^2\cdots\right)\\
v_L^* &= v_L\\
\rho_R^* &= \rho_{ref}\left(\rho_{R,0} + M_*\left(\rho_{R,1} - \rho_{R,0}\frac{\sqrt{\rho_{L,0}\rho_{R,0}}}{\sqrt{\rho_{L,0}}+\sqrt{\rho_{R,0}}}\frac{\Delta u_1}{\sqrt{\gamma p_0}} + \frac{\rho_{R,0}\sqrt{\rho_{R,0}}}{\sqrt{\rho_{L,0}}+\sqrt{\rho_{R,0}}}\frac{\Delta p_1}{\gamma p_0}\right) + M_*^2\cdots\right)\\
v_R^* &= v_R
\end{aligned} \tag{A.4}$$

Consider now the application of Godunov scheme in a Finite Volume framework. For simplicity, we consider that we use a regular Cartesian grid of uniform mesh size δ in two dimensions. $\boldsymbol{i} = (i,j)$ is the index of the node whose coordinates are $(i\delta, j\delta)$ and we use the notation $\mathscr{V}(\boldsymbol{i}) = \{(i-1,j),(i+1,j),(i,j-1),(i,j+1)\}$ or $\mathscr{V}(\boldsymbol{i}) = \{N,S,E,W\}$ for labeling the neighbors of the grid node $\boldsymbol{i}$. The cell associated with node $\boldsymbol{i}$ is $C_{\boldsymbol{i}} = [(i-1/2)\delta,(i+1/2)\delta]\times[(j-1/2)\delta,(j+1/2)\delta]$, $\vec{n}$ is the outward unit normal vector on $\partial C_{\boldsymbol{i}}$ and we note $\vec{n}_{\boldsymbol{il}} = \int_{C_{\boldsymbol{i}}\cap C_{\boldsymbol{l}}}\vec{n}/\delta$.

When a steady state is reached, the application of a first-order finite volume scheme yields the following semi-discrete equation:

$$\sum_{\boldsymbol{l}\in\mathscr{V}(\boldsymbol{i})}\vec{F}(q_{\boldsymbol{il}})\cdot\vec{n}_{\boldsymbol{il}} = 0 \tag{A.5}$$

where $q_{\boldsymbol{il}}$ denote the value of the state on the interfaces between the cells $\boldsymbol{i}$ and $\boldsymbol{l}$. Following the analysis that we have performed on the asymptotic solution of the Riemann problem, we write these interface values in the following form:

$$\begin{aligned}
\rho_{\boldsymbol{il}} &= \rho_{ref}(\rho^0_{\boldsymbol{il}} + M_*\rho^1_{\boldsymbol{il}} + M_*^2\rho^2_{\boldsymbol{il}} + \cdots)\\
u_{\boldsymbol{il}} &= a_{ref}(0 + M_* u^1_{\boldsymbol{il}} + M_*^2 u^2_{\boldsymbol{il}} + \cdots)\\
v_{\boldsymbol{il}} &= a_{ref}(0 + M_* v^1_{\boldsymbol{il}} + M_*^2 v^2_{\boldsymbol{il}} + \cdots)\\
p_{\boldsymbol{il}} &= \rho_{ref}a^2_{ref}(p^0_{\boldsymbol{il}} + M_* p^1_{\boldsymbol{il}} + M_*^2 p^2_{\boldsymbol{il}} + \cdots)
\end{aligned} \tag{A.6}$$

then the flux function evaluated on this state has the following expansion (here $u_{\boldsymbol{il}}, v_{\boldsymbol{il}}$ denote respectively the normal and tangential velocities on the interface):

$$\begin{aligned}
(\vec{F}(q_{\boldsymbol{il}})\cdot\vec{n}_{\boldsymbol{il}})_1 &= \rho_{ref}a_{ref}(M_*\rho^0_{\boldsymbol{il}}u^1_{\boldsymbol{il}} + \mathscr{O}(M_*^2))\\
(\vec{F}(q_{\boldsymbol{il}})\cdot\vec{n}_{\boldsymbol{il}})_2 &= \rho_{ref}a^2_{ref}(p^0_{\boldsymbol{il}} + M_* p^1_{\boldsymbol{il}} + M_*^2(\rho^0_{\boldsymbol{il}}(u^1_{\boldsymbol{il}})^2 + p^2_{\boldsymbol{il}}) + \mathscr{O}(M_*^3))\\
(\vec{F}(q_{\boldsymbol{il}})\cdot\vec{n}_{\boldsymbol{il}})_3 &= \rho_{ref}a^2_{ref}(M_*^2\rho^0_{\boldsymbol{il}}u^1_{\boldsymbol{il}}v^1_{\boldsymbol{il}} + \mathscr{O}(M_*^3))\\
(\vec{F}(q_{\boldsymbol{il}})\cdot\vec{n}_{\boldsymbol{il}})_4 &= \rho_{ref}a^3_{ref}\left(M_*\frac{\gamma}{\gamma-1}p^0_{\boldsymbol{il}}u^1_{\boldsymbol{il}} + \mathscr{O}(M_*^2)\right)
\end{aligned}$$

From the expression (A.3) of the interface pressure, it is seen that $p^0_{il} = p^0 \,\forall il$. Then the order 0 momentum equations degenerates into

$$p^0 \sum_{l \in \mathscr{V}(i)} \vec{n}_{il} = 0$$

but the order M_* momentum equations are

$$\sum_{l \in \mathscr{V}(i)} p^1_{il} \vec{n}_{il} = 0 \tag{A.7}$$

where the value of p^1_{il} is given in (A.3). This gives for the horizontal momentum equation

$$-\frac{\sqrt{\rho^0_i} p^1_{\mathrm{W}} + \sqrt{\rho^0_{\mathrm{W}}} p^1_i}{\sqrt{\rho^0_i} + \sqrt{\rho^0_{\mathrm{W}}}} + \frac{\sqrt{\rho^0_{\mathrm{E}}} p^1_i + \sqrt{\rho^0_i} p^1_{\mathrm{E}}}{\sqrt{\rho^0_i} + \sqrt{\rho^0_{\mathrm{E}}}} = \sqrt{\gamma p^0} \left(\frac{\sqrt{\rho^0_i \rho^0_{\mathrm{E}}}}{\sqrt{\rho^0_i} + \sqrt{\rho^0_{\mathrm{E}}}} \Delta_{\mathrm{E}i}\, u^1 - \frac{\sqrt{\rho^0_i \rho^0_{\mathrm{W}}}}{\sqrt{\rho^0_i} + \sqrt{\rho^0_{\mathrm{W}}}} \Delta_{i\mathrm{W}} u^1 \right) \tag{A.8}$$

and a similar expression for the vertical momentum equation. From (A.8), it is clear that p^1 does not vanish as soon as the velocity field is not uniform. Note also that Eq. (A.8) is almost identical to the equation obtained for Roe discretization in [7].

References

[1] Bijl H, Wesseling P. A unified method for computing incompressible and compressible flows in boundary fitted coordinate. J Comput Phys 1998;141:153–73.

[2] Clerc S. Numerical simulation of the homogeneous equilibrium for two-phase flows. J Comput Phys 2000;161:354–75.

[3] Dervieux A, Guezengar D, Guillard H, Viozat C. Analysis of low Mach simulations with compressible upwind codes. In: ECCOMAS 98. John Wiley and Sons; 1998.

[4] Radespiel R, Turkel E, Kroll N. Assessment of preconditioning methods for multidimensional aerodynamics. Comput Fluids 1997;26:613–34.

[5] Grenier E. Oscillatory perturbations of the Navier–Stokes equations. J Math Pures Appl 1997;76:477–98.

[6] Guillard H, Abgrall R. Modélisation des fluides numériques compressibles. In: Series in Applied Mathematics, vol. 5. Paris: Gauthier-Villars/North Holland; 2001.

[7] Guillard H, Viozat C. On the behavior of upwind schemes in the low Mach number limit. Comput Fluids 1999;28:63–96.

[8] Klainerman S, Majda A. Compressible and incompressible fluids. Commun Pure Appl Math 1982;35:629–53.

[9] Klein R. Semi-implicit extension of a Godunov-type scheme based on low Mach number asymptotics I: One-dimensional flow. J Comput Phys 1995;121:213–37.

[10] Kreiss H-O. Problems with different time scales for partial differential equations. Commun Pure Appl Math 1980;33:399–440.

[11] Masella JM, Faille I, Galouët T. On an approximate Godunov scheme. Int J Comput Fluid Dyn 1999;12:133–49.

[12] Metivier G, Schochet S. The incompressible limit of the nonisentropic Euler equations. Arch Rat Mech Anal 2001;158:61–90.

[13] Metivier G, Schochet S. Limite incompressible des équations d'Euler non-isentropiques. Séminaire équations aux dérivées partielles de l'école Polytechnique, 2001. Available from: http://www.maths.univ-rennes1.fr/metivier/preprints.html.

[14] Paillère H, Clerc S, Viozat C, Toumi I, Magnaud J-P. Numerical methods for low Mach number thermal-hydraulic flows. In: ECCOMAS 98. John Wiley and Sons; 1998.
[15] Paillère H, Viozat C, Kumbaro A, Toumi I. Comparison of low Mach number models for natural convection problems. In: Eurotherm Seminar No 63. Genoa, Italy, 6–8 September 1999.
[16] Schall E, Viozat C, Koobus B, Dervieux A. On the computation of unsteady ans steady low Mach flows with implicit upwind methods. In: ECCOMAS 2001, 2001.
[17] Schochet S. Asymptotics for symmetric hyperbolic systems with a large parameter. J Differen Equat 1988;75:1–27.
[18] Schochet S. Fast singular limits of hyperbolic PDE's. J Differen Equat 1994;114:476–512.
[19] Toro EF. Riemann solvers and numerical methods for fluid dynamics. Berlin: Springer-Verlag; 1997.
[20] Turkel E. Preconditioned methods for solving the incompressible and low speed compressible equations. J Comput Phys 1987;72:277–98.
[21] Turkel E. Review of preconditioning methods for fluid dynamics. Appl Numer Math 1993;12:257–84.
[22] Turkel E. Preconditional techniques in computational fluid dynamics. Annu Rev Fluid Mech 1999:31–385.
[23] Turkel E, Fiterman A, van Leer B. Preconditioning and the limit of the compressible to the incompressible flow equations for finite difference schemes. Chichester: John Wiley and Sons; 1994. p. 215–34.
[24] Ukai S. The incompressible limit and the initial layer of the compressible Euler equations. J Math Kyoto Univ 1986;26:323–31.
[25] van Leer B, Darmofal D-L. Steady Euler solutions in O(n) operations. In: Vierendeels J, Dick E, Riemslagh K, editors. Multigrid Methods VI: Proceedings of the Sixth European Multigrid Conference, Gent, Belgium, 27–30 September 1999. Lect Notes Comput Sci Eng, vol. 14. Springer-Verlag; 2000. p. 24–33.
[26] Vierendeels J, Riemslagh K, Dick E. A multigrid semi-implicit line method for viscous incompressible and low-Mach number flows on high aspect ratio grid. J Comput Phys 1999;154:310–41.
[27] Viozat C. Calcul d'écoulements stationnaires et instationnaires à petit nombre de Mach et en maillages étirés. PhD thesis, University of Nice, Sophia, Antipolis, 1998.
[28] Viozat C. Calcul d'écoulements diphasiques dans une tuyère: Influence de la renormalisation du schéma de flux. Technical Report SYSCO/LGLS/RT/00-014, CEA, 2000.
[29] Volpe G. Performance of compressible flow codes at low Mach number. AIAA J 1993;31:49–56.
[30] Zienkiewicz OC, Szmelter J, Perraire J. Compressible and incompressible flows: an algorithm for all seasons. Comput Meth Appl Mech Eng 1990;78(1):105–21.